

Surface Impedance Model for Nano-scale Device Communications over an Interface

Dmitriy Penkin[†], Alexander Yarovoy[†] and Gerard Janssen^{*}

[†]*Microwave Sensing, Signals and Systems Group, Delft University of Technology, The Netherlands*

Email: D.Penkin@tudelft.nl; A.Yarovoy@ircr.tudelft.nl

^{*}*Wireless and Mobile Communications Group, Delft University of Technology, The Netherlands*

Email: G.J.M.Janssen@tudelft.nl

Abstract—To take into account the impact of an underlying half-space on the communication channel between nano-scale nodes, the surface-impedance-based model is proposed. To verify this approach, its results are compared to that of the singularity-based model developed for the particular half-space. Finally, by using the impedance-based approach, it is shown that the gain of the channel between nano-scale devices can be notably increased due to the contribution of surface waves.

Index Terms—Green’s function, nano-scale node, link power budget, channel gain, wireless nano-sensor network.

I. INTRODUCTION

Wireless sensor networks, composed of a multitude of autonomous nano-scale nodes with sensing, processing, and wireless communication capabilities, are envisioned to cause a revolution in the field of fine-grained environmental sensing and health monitoring [1]. These nano-sensor devices involved in Brownian motion may constantly and unpredictably move in an environment. Since it is of utmost importance to control the position of such devices to avoid long-term harmful effects (e.g. [2]), nano-nodes are initially envisioned to be tightly fixed on an underlying surface. Moreover, the resulting static network topology ensures that all sensed data will be correctly conveyed through the network.

As a consequence of their limited volume, the sensor nodes will operate on an extremely restricted energy budget [3]. In this way, it is crucial to reduce the power consumption of the devices to the level that meets the capabilities of a nano-node power supply. Since the energy cost related to the conventional data transmission at radio-frequency (RF) is much higher than the energy needed to perform processing and sensing tasks, the promising solution is to set up the communication between nano-nodes via surface waves (e.g. [4]). These waves only propagate along the interface between differing media and experience low attenuation along propagation paths compared to the space waves. Note that the issue of the exponential decrease of surface wave amplitude with depth can be avoided by the ability to place nano-nodes very close to the interface. Last but not least, to the authors’ knowledge, such a surface influence has not been considered for communication between nano-devices so far.

Typically, to develop a mathematical model capable of calculating the contribution of surface waves is a formidable

task as well as this model can be used for a particular geometry of underlying half-space. In this regard, when it is possible to define a surface impedance Z_s , which stands for the ratio between the tangential electric and magnetic fields on the surface, this can essentially facilitate the solution of an electromagnetic boundary-value problem in the communication medium as there is no need to examine in detail the fields in the bottom half-space. In particular, since nano-nodes behave as point source radiators due to their size limitations, the surface-wave influence can be estimated in a straightforward manner by applying the Green’s function for a point source above a half-space, introduced by Felsen and Marcuvitz in [5]: the authors incorporate the impact of the bottom half-space into their model through its surface impedance value Z_s .

In general, the surface impedance is formally determined for the case of a normally incident plane wave. Since nano-nodes are situated close to an interface as well as the value of Z_s depends on an incident wave number, the aim of this paper is to verify the possibility to apply the typical Z_s for properly evaluating the surface wave contribution in the event of a grazing incident wave. Meanwhile, the other goal is to expand the applicability limits of the asymptotic expression for the above Green’s function by comparing its results with that of an singularity-based approach. Another objective is to indicate the performance enhancement of the channel between nano-scale devices due to the contribution of surface waves.

This paper is organized as follows. The surface-impedance-based model capable of calculating the power budget of the channel between nano-nodes placed above a bottom lossy half-space is shown in Section II, whereas the singularity-based method is developed in Section III. To broaden the applicability of the impedance-based model, the comparison analysis of these two approaches is accomplished

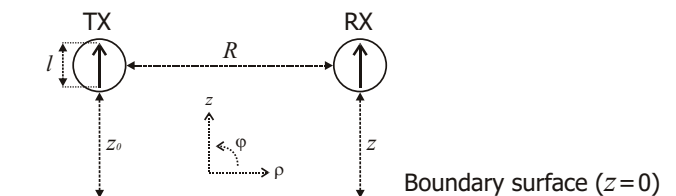


Fig. 1. One-hop communication channel between nano-nodes located above a bottom half-space.

in Section IV. The impact of surface waves on the channel between nano-scale devices is assessed in Section V. Finally, conclusions are given in Section VI.

II. SURFACE-IMPEDANCE-BASED MODEL

A. System model

In the paper, we calculate the power budget of a basic communication system between transmitting (TX) and receiving (RX) nano-nodes operating in free half-space with parameters $\varepsilon_0 = (36\pi)^{-1} \times 10^{-9}$ F/m and $\mu_0 = 4\pi \times 10^{-7}$ H/m in the presence of a bottom half-space (Fig.1). Both TX and RX devices are located above this interface and equipped with antennas of dimension l for performing signal transmissions via RF waves. Note that other node components as well as a material to fix the node to the surface are assumed to possess negligible impact on the one-hop channel due to their small dimensions with respect to the wavelength λ . Also, the surface is considered to be perfectly flat and non-curved. The antenna element is electrically very small ($l \ll \lambda$) and acts as a Hertzian electric dipole as a consequence of the node size restrictions. The polarization of the antenna is considered to be vertical because it is subject to considerably less attenuation than horizontally polarised signals. Eventually, the cylindrical coordinate system is used to define the positions of the nodes.

For the numerical simulations below, each nano-node is assumed to be equipped with a vertical dipole antenna of length $l = \lambda/100$. The nodes are placed above the boundary surface at the height $z_0 = z = \lambda/10$ and the output power is considered to be the same. The operating frequency is set to 10 GHz.

The power budget analysis is performed here based on the Green's function formalism. In this respect, the field strength at an observation point is treated in terms of the integral of the Green's function multiplied by a current density on the transmitting antenna. This current density for an electrically very small dipole is in particular assumed to be one-dimensional and triangularly distributed over the antenna aperture [6]:

$$\vec{j}^e(\rho', \varphi', z') = A \left(1 - \frac{|z' - z_0|}{l/2} \right) \frac{\delta(\rho' - \rho_0)}{\rho_0} \delta(\varphi' - \varphi_0) \vec{z}^o, \quad (1)$$

where \vec{z}^o is the unit direction vector of the dipole current. The TX antenna is fed by an ideal source of frequency f with source amplitude A , (ρ_0, φ_0, z_0) are the coordinates of the dipole center and point z' belongs to the antenna aperture (i.e., $z' \in [z_0 - l/2; z_0 + l/2]$). Since the dipole is approximated as a point source radiator, the magnitude of the current density at this point is given by the following expression:

$$\left| \vec{j}^e(\rho_0, \varphi_0, z_0) \right| = \int_{z_0 - l/2}^{z_0 + l/2} A \left(1 - \frac{|z' - z_0|}{l/2} \right) dz' = \frac{Al}{2}. \quad (2)$$

The electric field at an arbitrary observation point (ρ, φ, z) resulting from a point source is obtained through the Hertz potential as:

$$\vec{E}(\rho, \varphi, z) = [\text{grad div} + k^2] \vec{Z}^e(\rho, \varphi, z), \quad (3)$$

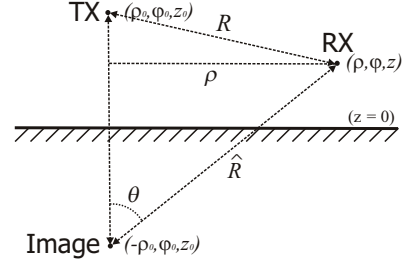


Fig. 2. The point source radiator above the bottom half-space.

where $k = 2\pi\sqrt{\varepsilon\mu}/\lambda$ is the wavenumber (for free space it corresponds to $k_0 = 2\pi/\lambda$) and $\vec{Z}^e(x, y, z)$ is the Hertz vector. The solution for this vector is known (e.g. [5]) and given by:

$$\vec{Z}^e(\rho, \varphi, z) = \frac{1}{4\pi i \omega \varepsilon} \times \int_V \vec{j}^e(\rho_0, \varphi_0, z_0) G^e(\rho, \varphi, z, \rho_0, \varphi_0, z_0) d\rho d\varphi dz, \quad (4)$$

where $\omega = 2\pi f$ corresponds to the angular frequency, i is the imaginary unit and G^e stands for the Green's function.

The magnitude of induced current on the RX antenna is obtained by assuming that this current is triangularly distributed on the electrically small dipole:

$$I = \frac{1}{Z_0 + Z_l} \int_{z'' - l/2}^{z'' + l/2} E_\tau \left(1 - \frac{|z'' - z|}{l/2} \right) dz'', \quad (5)$$

where z is the Z -coordinate of the point-source RX dipole, Z_0 and Z_l are the complex impedances of the antenna and the receiver circuit, respectively. E_τ is the projection of \vec{E} from Eq.(3) onto the vector $\vec{\tau}$ representing the direction of the receiving dipole. Since here both TX and RX antennas are vertically polarized, the value of E_τ is equal to $|\vec{E}|$.

The power available to a RX electronic circuit is given by:

$$p = \frac{|I|^2 \text{Re}(Z_l)}{2}. \quad (6)$$

Let us further focus on the maximum value of p assuming that there are no losses between the RX dipole and the electronic circuit (i.e., $Z_l = Z_0^*$). Thus, taking into account the above equations, the final expression for p can be rewritten as:

$$p = \frac{l^2 |E|^2}{8 \text{Re}(Z_0)} = \frac{225 l^4 A^2}{8 k^2 \text{Re}(Z_0)} \cdot \left| \left[\frac{\partial^2}{\partial z^2} + k^2 \right] G^e(\rho, \varphi, z, \rho_0, \varphi_0, z_0) \right|^2. \quad (7)$$

Note that partial differentiation is performed only with respect to z as both the antennas are aligned along the Z -axis. Eventually, as can be seen from Eq.(7), the magnitude of p can be estimated at any space point if the Green's function can be constructed for this particular electrodynamic volume.

B. Impedance-based Green's function

Based on the surface impedance concept, the Green's function for arbitrary distances R from the source in the region $z > 0$ has been evaluated in [5] and has the following form:

$$G^e(\rho, \varphi, z, \rho_0, \varphi_0, z_0) = \frac{e^{-ikR}}{4\pi R} - \frac{\bar{Z}_s - \cos\theta}{\bar{Z}_s + \cos\theta} \cdot \frac{e^{-ik\hat{R}}}{4\pi\hat{R}} - \bar{Z}_s \sqrt{\frac{1}{\lambda\rho}} \left(\frac{e^{-i\pi}}{1 - \bar{Z}_s^2} \right)^{\frac{1}{4}} e^{-ik\sqrt{1 - \bar{Z}_s^2}\rho} e^{ik\bar{Z}_s(z_0+z)} U(\theta - \theta_p), \quad (8)$$

where $\bar{Z}_s = Z_s/\sqrt{\mu_0/\varepsilon_0} \approx Z_s/120\pi$ is the normalized impedance and $\theta = \arcsin(\rho/\hat{R})$ is the observation angle (Fig.2). The Heaviside step function $U(\theta - \theta_p)$ contributes only if θ exceeds $\theta_p = \text{Re}(\Omega_p) - \arccos(\text{sech}(\text{Im}(\Omega_p)))$, where $\cos\Omega_p = -\bar{Z}_s$. The first and the second term on the right-hand side of Eq.(8) corresponds to the free-space Green's function for the unbounded region and the contribution of waves reflected from the interface, respectively. In other words, these terms constitute the geometric optical fields, whereas the third component comprises the surface waves which contribute only when $\theta > \theta_p$. Note that the latter component can only asymptotically estimate the influence of surface waves since the absence of their residue terms (i.e., when $\theta < \theta_p$) does not imply the non-existence of surface waves but merely indicates that their amplitudes are beyond the approximation. Due to the fact that the decay of the surface waves ($\sim 1/\sqrt{\rho}$) is slower than that of the direct ($\sim 1/R$) and reflected waves ($\sim 1/\hat{R}$), the surface waves may cause a dominant contribution at a receiver and, thus, it is of importance to estimate their impact for any arbitrary distance R (i.e., any observation angle θ). In this regard, we specify a particular geometry for the bottom half-space and calculate the surface-wave contribution in two ways: (1) by using the Green's function from Eq.(8) in which the Heaviside step function is neglected; (2) by applying expressions derived based on a singularity-based model. Next, from the comparative analysis of results coming from both approaches, the surface-impedance-based model has to be verified as well as its applicability limits might be expanded.

The bottom half-space, representing a commonly used substrate for antenna configurations, is further used for our simulations. In particular, it consists of a thin layer of thickness b coated on a thick ideal metal (Fig.3). The material of the thin layer is lossy dielectric with parameters $(\varepsilon_g, \mu = 1)$.

C. Impedance of dielectric film covering thick metal

In order to use the surface-impedance-based concept, it is required to know the specific value of \bar{Z}_s for a given half-space geometry. In this respect, we consider the model of a plane electromagnetic wave normally incident on a dielectric layer with complex dielectric constant ε_g and magnetic permeability $\mu_g = \mu_0$. By taking care of the boundary conditions for the electromagnetic field components on both surfaces of the dielectric layer, the boundary-value problem is treated. By adopting the criteria of impedance boundary condition at the

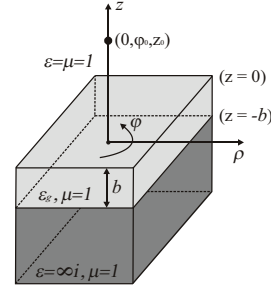


Fig. 3. The lossy dielectric film of thickness b coated on a thick metal.

top of the dielectric film, the mathematical expression for a distributed surface impedance \bar{Z}_s is given by the following:

$$\bar{Z}_s = i(\mu_g/\varepsilon_g)^{1/2} \tan(k_g b), \quad (9)$$

where $k_g = 2\pi\sqrt{\varepsilon_g\mu_g}/\lambda$ is the wavenumber in the dielectric layer. Note that although the value of \bar{Z}_s was determined for the event of a normally incident wave, it will be seen from the comparative analysis that Eq.(9) is applicable to determine the distributed impedance in the case of a grazing incident wave.

Next, the lossy carbon is taken as a reference because this material as well as its composites are widely utilized. Thus, its dielectric constant $\varepsilon_g = 15 - 8i$ is extracted from [7] at the operating frequency $f = 10$ GHz and, eventually, the value \bar{Z}_s as a function of the thickness b is shown in Fig.4.

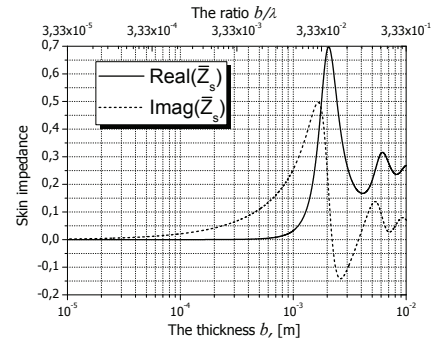


Fig. 4. The distributed impedance of carbon film on the ideal metal.

According to Shevchenko [8], the contribution of surface waves qualitatively changes with varying impedance value: in particular, to provide the surface with directive properties, \bar{Z}_s has to be inductive with a positive imaginary part. In turn, the larger the non-zero real part of \bar{Z}_s , the higher are the losses in the boundary layer. Therefore, we can conclude that the surface-wave contribution is more considerable for the surface impedance value characterized by a lower real part as well as a higher inductivity. In this respect, a substantial surface wave contribution is expected at $b \approx 10^{-3}$ m as the corresponding impedance \bar{Z}_s possesses such features (Fig.4).

III. SINGULARITY-BASED METHOD

As shown in [5], the circular waveguide representation of the Green's function $G(\vec{r}, \vec{r}_0)$ for vertical Hertzian electric

dipole located on the z axis (i.e., $\rho_0 = 0$) is given by:

$$G(\rho, \varphi, z, 0, \varphi_0, z_0) = \frac{1}{4\pi} \int_{-\infty}^{\infty} \varkappa H_0^{(2)}(\varkappa \rho) g(z, z_0) d\varkappa, \quad (10)$$

where \varkappa is complex transverse wavenumber, $H_0^{(2)}$ stands for the Hankel function of the second kind and zero order, whilst $g(z, z_0)$ is the one-dimensional modal Green's function. Note that the pole singularities of the latter function are descriptive of the surface waves (i.e., the waves guided in the direction transverse to z). Since the longitudinal function $g(z, z_0)$ depends on the nature of z stratification, its representation is derived for the region given above (i.e., Fig.3). In particular, by adopting the boundary conditions for the electric fields on both surfaces of the dielectric film as well as the wave equations in free space and dielectric medium, the functional form of $g(z, z_0)$ is expressed as follows:

$$g(z, z_0) = \frac{4\pi \cdot e^{-i\gamma_1(z+z_0)}}{i\gamma_1 \varepsilon_g + \gamma_2 \tan(\gamma_2 d)}, \quad (11)$$

where $\gamma_1^2 = k_0^2 - \varkappa^2$ and $\gamma_2^2 = k_0^2 \varepsilon_g \mu_g - \varkappa^2 = k_g^2 - \varkappa^2$ is the longitudinal wavenumber in free space and dielectric region, respectively. In this way, the term in modulus in the final equation (7) can be represented as:

$$\begin{aligned} M &= \left[\frac{\partial^2}{\partial z^2} + k^2 \right] G^e(\rho, \varphi, z; 0, \varphi_0, z_0) = \\ &= \int_{-\infty}^{\infty} \frac{\varkappa^3 H_0^{(2)}(\varkappa \rho) e^{-i\gamma_1(z+z_0)}}{i\gamma_1 \varepsilon_g + \gamma_2 \tan(\gamma_2 d)} d\varkappa. \end{aligned} \quad (12)$$

As noted above, we have to extract and obtain exactly the residue contributions to determine the surface wave impact. Thus, the integral in Eq.(12) possesses simple poles which can be presented separately as:

$$\begin{aligned} M &= \int_{-\infty}^{\infty} \frac{\varkappa^3 H_0^{(2)}(\varkappa \rho) e^{-i\gamma_1(z+z_0)}}{i\gamma_1 \varepsilon_g + \gamma_2 \tan(\gamma_2 d)} d\varkappa + \\ &+ 2\pi i \sum_{n=1}^N \lim_{\varkappa \rightarrow \varkappa_n} \left[(\varkappa - \varkappa_n) \frac{\varkappa^3 H_0^{(2)}(\varkappa \rho) e^{-i\gamma_1(z+z_0)}}{i\gamma_1 \varepsilon_g + \gamma_2 \tan(\gamma_2 d)} \right]. \end{aligned} \quad (13)$$

The underlined lower integration limit indicates that the singularity points are avoided: hence, the integral on the right-hand side corresponds to the contribution of geometric optical fields, whereas the sum stands for the influence of surface waves. The latter term is reconstituted by means of the standard algebraic method and the expression for M is given by:

$$\begin{aligned} M &= \int_{-\infty}^{\infty} \frac{\varkappa^3 H_0^{(2)}(\varkappa \rho) e^{-i\gamma_1(z+z_0)}}{i\gamma_1 \varepsilon_g + \gamma_2 \tan(\gamma_2 d)} d\varkappa - \\ &- \sum_{n=1}^N \frac{2\pi \varkappa_n^2 H_0^{(2)}(\varkappa_n \rho) e^{-i\gamma_{1n}(z+z_0)}}{\varepsilon_g \cos^2(\gamma_{2n} d) + \frac{\tan(\gamma_{2n} d)}{\gamma_{2n} \varepsilon_g} - \frac{i}{\gamma_{1n}}}. \end{aligned} \quad (14)$$

Hence, the contribution of surface waves is shown in explicit form and can be evaluated if the pole singularities \varkappa_n are determined. Evidently, these singularities are roots of the dispersive equation which is also the denominator of M :

$$i\gamma_1 \varepsilon_g + \gamma_2 \tan(\gamma_2 d) = 0. \quad (15)$$

IV. COMPARATIVE ANALYSIS

A. Analysis of dispersive equation

To be able to use the singularity-based model, the roots of the dispersive equation need to be evaluated first [9]. As this transcendental equation is unable to be treated analytically, it is solved in a graphical manner. In the course of its evaluation, we can conclude the following: (1) each solution \varkappa_n corresponds to the transverse wavenumber of the respective surface wave mode and its value lies in the range $k_0 < \varkappa_n < k_g$; (2) the higher are the operating frequency f , the thickness of dielectric film b and the dielectric constant ε_g , the higher is the total number of surface modes to propagate; (3) there is at least one surface mode presented in the given bottom half-space.

B. Single-mode scenario

As stated above, in a very thin dielectric film only the single/fundamental surface mode can propagate. Upon further analysis of the single-solution case, it was discovered that its transverse wavenumber is always associated with the surface impedance and straightforwardly approximated as $\varkappa_n^{(1)} = k_0 \sqrt{1 - Z_g^2}$. In particular, the contribution of the fundamental mode for fixed b is demonstrated in Fig.5, where

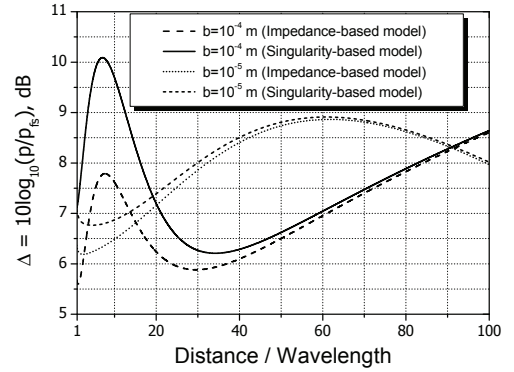


Fig. 5. The ratio $\Delta = 10 \log_{10}(p/p_{fs})$ when thickness b is small.

we compare the received power p in the presence of the half-space with that obtained in free space (hereinafter denoted as p_{fs}). Since the geometric optical impact is known to not exceed 6 dB level, the surface wave constructively interferes. As can be also seen in Fig.5, the difference between two models increases when the communication distance decreases. Nonetheless, since the impedance-based model is envisioned to be a lower-bound estimate of p , at the first approximation we can neglect the Heaviside step function in Eq.(8) to be able to calculate the surface wave contribution for short distances R (in particular, for $b = 10^{-5}$ m by using Eq.(8) the surface wave contribution is estimated to be non-zero only when $R > 95\lambda$).

C. Multi-mode scenario

The growing number of surface modes can propagate within the dielectric film with increasing its thickness. For example, about thirty surface modes excluding the fundamental one exist in the carbon film of thickness $b = 10$ cm (Fig.6). However, as can be seen from the second

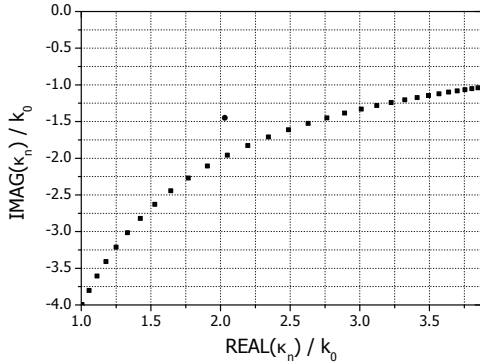


Fig. 6. Roots of the dispersive equation (15) when thickness $b = 10$ cm.

term on the right-hand side of Eq.(14), none of these modes convey a substantial amount of energy to the free space: i.e., experiencing internal reflections they can propagate within the dielectric slab solely. Meanwhile, the fundamental surface mode decays with increasing the thickness b : i.e., it loses energy due to a growing number of higher surface modes in the slab. In particular, since the transverse wavenumber of the fundamental surface wave $\kappa_n^{(1)}$, indicated by the circle in Fig.6, possesses both large real and imaginary parts, the amplitude of this mode is very minute. Therefore, in the case of the multi-mode scenario, a negligibly small contribution of surface waves can come to a receiver located in free space.

The same result (i.e., the almost zero impact of surface waves) is also envisioned by applying the impedance-based approach. In particular, starting from $b = 10^{-3}$ m the real part of \bar{Z}_s , which is responsible for the losses in the dielectric layer, is relatively large. Put differently, the energy got into the dielectric film of large thickness is merely used for heating this slab rather than propagating to free space.

V. NUMERICAL ANALYSIS OF SURFACE WAVE IMPACT

Since the surface-impedance-based method has been shown to properly model the impact of surface waves, to bridge the gap between power demands of nano-scale node and capabilities of its energy unit, the maximum potential contribution of surface waves is further determined by means of this approach. In other words, the value $\Delta = 10 \log_{10}(p/p_{fs})$ is computed by specifying the surface impedance factor but not the bottom half-space geometry. Thus, to prevent the absorption of energy by the dielectric layer the real part of \bar{Z}_s is set to zero, whilst its imaginary part changes from low to high values. As can be seen in Fig.7, the contribution of surface waves is indeed maximised when the imaginary part is large. In particular, at big communication distances R , the channel gain can be increased up to 30 dB due to the implementation of the

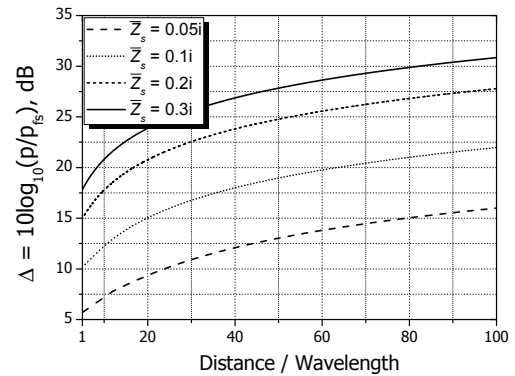


Fig. 7. The ratio $\Delta = 10 \log_{10}(p/p_{fs})$ for the bottom half-spaces characterized by pure imaginary values of surface impedance.

specific bottom half-space. For comparison, in the case of the carbon film of thickness $b = 5 \cdot 10^{-4}$ m coated on the thick metal ($\bar{Z}_s = 0.004 + 0.111i$, Fig.4), the channel gain at $R = 100\lambda$ is about 20 dB.

VI. CONCLUSION

The channel power budget model has been developed based on the surface impedance factor. Such a model notably simplifies the electromagnetic problem as there is no need to take care of fields within the bottom half-space. To test the feasibility of this impedance-based approach, the analytical singularity-based framework has been also built for the particular geometry of the bottom half-space. The comparative analysis of both the approaches has not only verified the impedance-based concept but also expanded its applicability limits. Eventually, by applying the impedance-based model, the gain of the peer-to-peer channel between nano-scale devices has been shown to significantly increase. In particular, the possibility to enhance this gain up to 30 dB due to the implementation of the specific half-space has been demonstrated.

REFERENCES

- [1] M. Ilyas and I. Mahgoub, *Smart Dust: Sensor Network Applications, Architecture and Design*. CRC Press, 2006.
- [2] C. A. Poland, R. Duffin, I. Kinloch, A. Maynard, W. A. H. Wallace, A. Seaton, V. Stone, and S. Brown, "Carbon nanotubes introduced into the abdominal cavity of mice show asbestos-like pathogenicity in a pilot study." *Nature nanotechnology*, vol. 3, pp. 423–8, 2008.
- [3] S. Roundy, D. Steingart, L. Frechette, P. K. Wright, and J. M. Rabaey, "Power Sources for Wireless Sensor Networks," in *EWSN'04*, pp. 1–17.
- [4] Y. P. Zhang, Z. M. Chen, and M. Sun, "Propagation mechanisms of radio waves over intra-chip channels with integrated antennas: Frequency-domain measurements and time-domain analysis," *Antennas and Propagation, IEEE Transactions on*, 2007.
- [5] L. Felsen and N. Marcuvitz, *Radiation and Scattering of Waves*, ser. IEEE Press Series on Electromagnetic Waves. IEEE Press, 1994.
- [6] R. King and G. Smith, *Antennas in Matter: Fundamentals, Theory, and Applications*. Mit Press, 1981.
- [7] M. Hotta, M. Hayashi, M. Lanagan, D. Agrawal, and K. Nagata, "Complex permittivity of graphite, carbon black and coal powders in the ranges of x-band frequencies (8.2 to 12.4 ghz) and between 1 and 10 ghz," vol. 51, no. 11, pp. 1766–1772, 11 2011.
- [8] V. Shevchenko, *Continuous transitions in open waveguides: introduction to the theory*, ser. Golem series in electromagnetics. Golem Press, 1971.
- [9] L. Vaynshteyn, *Open resonators and open waveguides*, ser. The Golem series in electromagnetics. Golem Press, 1969.